

Superfluid and Mott Insulating shells of bosons in harmonically confined optical lattices

Kaushik Mitra, C. J. Williams and C. A. R. Sá de Melo

*Joint Quantum Institute
University of Maryland, College Park, MD 20742
NIST, Gaithersburg, MD 20899*

(Dated: August 21, 2021)

Weakly interacting atomic or molecular bosons in quantum degenerate regime and trapped in harmonically confined optical lattices, exhibit a wedding cake structure consisting of insulating (Mott) shells. It is shown that superfluid regions emerge between Mott shells as a result of fluctuations due to finite hopping. It is found that the order parameter equation in the superfluid regions is not of the Gross-Pitaevskii type except near the insulator to superfluid boundaries. The excitation spectra in the Mott and superfluid regions are obtained, and it is shown that the superfluid shells possess low energy sound modes with spatially dependent sound velocity described by a local index of refraction directly related to the local superfluid density. Lastly, the Berezinskii-Kosterlitz-Thouless transition and vortex-antivortex pairs are discussed in thin (wide) superfluid shells (rings) limited by three (two) dimensional Mott regions.

PACS numbers: 03.75.Hh, 03.75.Kk, 03.75.Lm

I. INTRODUCTION

The recent experimental discovery of Bose-Mott insulating phases in optical lattices has generated an explosion of research in the ultra-cold atom community (see [1] for a recent review), and has helped to merge two major branches of physics: atomic-molecular-optical and condensed matter physics. Most experiments thus far have relied on measuring the momentum distribution of the atoms after switching off the trap confining the atoms to infer the existence of a superfluid to insulator transition [2, 3, 4]. However, very recently, two experimental groups [5, 6] have used spatially selective microwave spectroscopy to probe *in situ* the superfluid-to-insulator transition of ^{87}Rb in a three dimensional (3D) optical lattice with a harmonic envelope. In these experiments, the shell structure of the Bose-Mott insulating states was revealed for very deep lattices. Regions of filling fraction $n = 1$ through $n = 5$ ($n = 1$ through $n = 3$) were mapped in the MIT [5] (Mainz [6]) experiment. Their observations in three-dimensional optical lattices lead to the confirmation of the Mott-insulating shell structure consisting of “Mott plateaus” with abrupt transitions between any two successive shells as proposed in two dimensional (2D) [7] optical lattices.

One of the next frontiers for ultra-cold bosons in optical lattices is the search for superfluid regions separating Mott-insulating shells. Eventhough the Mott shell structure was determined recently using microwave spectroscopy [5, 6], any evidence of superfluid shells has remained elusive. Thus, in anticipation of the next experimental breakthrough, we study 2D and 3D optical lattices of atomic or molecular bosons in harmonically confining potentials, and show that between the Mott regions of filling fraction n and $n + 1$, superfluid shells emerge as a result of fluctuations due to finite hopping, and extend our previous work on this topic [8]. This finite hop-

ping breaks the local energy degeneracy of neighboring Mott-shells, determines the size of the superfluid regions and is responsible for the low energy (sound) and vortex excitations. In addition, we find that the order parameter equation is not in general of the Gross-Pitaevskii type. Furthermore, in 3D optical lattices, when superfluid regions are thin (nearly 2D) spherical or ellipsoidal shells, we obtain bound vortex-antivortex excitations below the Berezinski-Kosterlitz-Thouless (BKT) transition temperature [9, 10] which is different for each superfluid region. Finally, we propose the use of Laguerre-Gaussian and Bragg spectroscopy techniques for the detection of superfluid shells.

The remainder of the manuscript is organized as follows. In Sec. II, we present the Bose-Hubbard Hamiltonian in a harmonic trap. In Sec. III, we analyze the emergence of an alternating superfluid and Mott shell structure, comparing two different approaches involving non-degenerate and nearly degenerate perturbation theory. We also obtain the order parameter equation, the characteristic sizes of the superfluid and Mott regions, the local filling fraction and the local compressibility. We find that the superfluid order parameter that emerges between two Mott shells is not of the Gross-Pitaevskii type, except very close to the insulating boundaries. In Sec. IV, we describe quasiparticle and quasihole excitations in the Mott regions and quasiparticle, sound and vortex excitations in the superfluid regions. In Sec. V, we present a possible experiment using Gauss-Laguerre beams and Bragg spectroscopy, which can be performed in order to visualize the existence of superfluid shells. Lastly, we state our conclusions in Sec. VI.

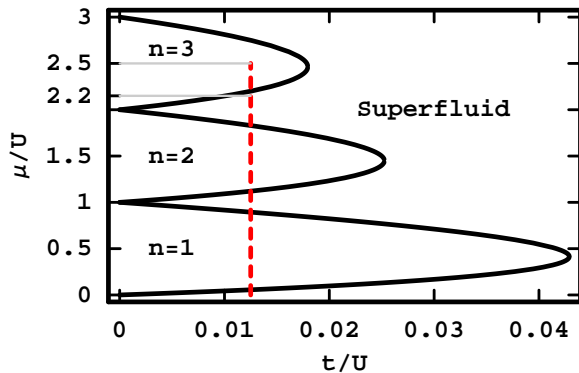


FIG. 1: (Color online) Phase diagram of the homogeneous Bose Hubbard model. For the inhomogeneous Bose Hubbard system, the dashed (red) line indicates the values of the local chemical potential $\mu_{\mathbf{r}}$ that the system exhibits from $\mu_{\mathbf{r}} = 2.5U$ (Fig 4) or $\mu_{\mathbf{r}} = 2.2U$ (Fig 5) at the center of the trap to $\mu_{\mathbf{r}} = 0$ at the edge of the trap for $t = 1.25 \times 10^{-2}U$. It indicates how the system exhibits an alternating structure of Mott and superfluid shells

II. BOSE-HUBBARD HAMILTONIAN

To describe the physics of alternating insulating and superfluid shells of atomic or molecular bosons in optical lattices, we use the lattice Bose-Hubbard Hamiltonian with a harmonic potential described by

$$H = -t \sum_{\mathbf{r}, \mathbf{a}} c_{\mathbf{r}}^{\dagger} c_{\mathbf{r}+\mathbf{a}} + \frac{U}{2} \sum_{\mathbf{r}} c_{\mathbf{r}}^{\dagger} c_{\mathbf{r}}^{\dagger} c_{\mathbf{r}} c_{\mathbf{r}} - \sum_{\mathbf{r}} \mu_{\mathbf{r}} c_{\mathbf{r}}^{\dagger} c_{\mathbf{r}} \quad (1)$$

where $\mu_{\mathbf{r}} = \mu - V(\mathbf{r})$ is the local chemical potential,

$$V(\mathbf{r}) = \Omega_{\rho}(\rho/a)^2/2 + \Omega_z(z/a)^2/2 \quad (2)$$

is the harmonically confining potential, a is the lattice spacing, and $c_{\mathbf{r}}^{\dagger}$ is the creation operator for a boson at site \mathbf{r} . Here, the vector $\mathbf{r} = (x, y, z)$, and the distance $\rho = \sqrt{x^2 + y^2}$. The anisotropic confining potential $V(\mathbf{r})$ becomes isotropic when $\Omega_{\rho} = \Omega_z$. Furthermore, t is the hopping parameter and U is the interaction strength, which we assume to be repulsive (positive). The sum in the first term on the right hand side of Eq. 1 is restricted to nearest neighbors. The harmonic trap makes the system inhomogeneous and introduces interesting properties which are absent in homogeneous Bose-Hubbard systems [11, 12]. For the inhomogeneous systems, it is useful to define a local chemical potential $\mu_{\mathbf{r}} = \mu - V(\mathbf{r})$ which plays an essential role in the emergence of shell structures.

For bosons in a homogeneous optical lattice, the Bose-Hubbard model without the harmonic confining potential can be used. In this case, it is well known that an integer number of particles on each site or $\mathbf{r} + \mathbf{a}$ describes an insulating state for sufficiently large U ($U \gg t$). This is because the on-site interaction U makes it energetically

unfavorable for a particle to move from one site to another. In this situation the system is in what is known as the Mott insulator phase [13]. However, for non-integer number of particle, the extra bosons can move more easily, at a small energy cost, because its interaction energy is essentially the same on every site. For this reason, a system with non-integer number of bosons on each site is a superfluid at zero temperature [11]. Recently, several Mott-insulator shells of bosons were detected in optical lattices [5, 6], which are inevitably inhomogeneous, and thus require a model that includes the effects of the harmonic part of the confining potential. This can be modeled by the inhomogeneous Bose-Hubbard hamiltonian described in Eq. (1). In this case, one can either be in a regime where the entire system is superfluid or in a regime where the system exhibits a shell structure of alternating Mott-insulator and superfluid regions. The existence of this shell structure has been shown numerically [7], but the lack of analytical progress has hindered a true understanding of the emergence and properties of these shells.

A simple argument for the emergence of the shell structure can be made by inspection of the standard phase diagram of the homogeneous Bose-Hubbard model shown in Fig. 1 upon the substitution of $\mu \rightarrow \mu_{\mathbf{r}}$. In an inhomogeneous system, the effective local chemical potential $\mu_{\mathbf{r}}$ is spatially varying. Thus, in the regions where the number density $n(\mathbf{r})$ is not an integer, a superfluid shell emerges, and in the regions where $n(\mathbf{r})$ is an integer, a Mott-insulator shell appears. Eventhough, a simple argument for the existence of the shell structure can be made, many questions need to be seriously addressed. For instance, what are the characteristic order parameter, dimensions and excitations of each superfluid shell? Thus, we begin our presentation by discussing next the emergence of the Mott-insulator and superfluid shell structure.

III. EMERGENCE OF THE SHELL STRUCTURE

A standard approach to analyse such bosonic systems is to use the Bogoliubov mean field approximation. However, as shown in [12], this approximation fails to predict the expected phase transition since it treats the interactions only approximately. Hence, instead of using the Bogoliubov approximation, we generalize a method found in the literature [11, 12], by introducing a local mean field theory that treats the interactions exactly and approximates the kinetic energy of the atoms in the optical lattice. We introduce the local superfluid order parameter $\psi_{\mathbf{r}} = \langle c_{\mathbf{r}} \rangle$. We can now construct a consistent local mean field theory by substituting the operator $c_{\mathbf{r}}^{\dagger} c_{\mathbf{r}+\mathbf{a}} \rightarrow \langle c_{\mathbf{r}}^{\dagger} \rangle c_{\mathbf{r}+\mathbf{a}} + c_{\mathbf{r}}^{\dagger} \langle c_{\mathbf{r}+\mathbf{a}} \rangle - \langle c_{\mathbf{r}}^{\dagger} \rangle \langle c_{\mathbf{r}+\mathbf{a}} \rangle$, leading to an effective local Hamiltonian

$$H_{\mathbf{r}}^{\text{eff}} = H_{0,n}(\mathbf{r}) - t \sum_{\mathbf{a}} (c_{\mathbf{r}} \psi_{\mathbf{r}+\mathbf{a}}^* + c_{\mathbf{r}}^{\dagger} \psi_{\mathbf{r}+\mathbf{a}} - \psi_{\mathbf{r}}^* \psi_{\mathbf{r}+\mathbf{a}}), \quad (3)$$

which is diagonal in the site index \mathbf{r} with

$$H_{0,n}(\mathbf{r}) = \frac{U}{2}\hat{n}_{\mathbf{r}}(\hat{n}_{\mathbf{r}} - 1) - \mu_{\mathbf{r}}\hat{n}_{\mathbf{r}}, \quad (4)$$

where $\hat{n}_{\mathbf{r}} = c_{\mathbf{r}}^\dagger c_{\mathbf{r}}$ is the number operator. For $t = 0$, the shell structure for Mott-insulating phases is revealed by fixing $\hat{n}_{\mathbf{r}} = n$, to obtain the local energy

$$E_{0,n}(\mathbf{r}) = \frac{U}{2}n(n-1) - \mu_{\mathbf{r}}n, \quad (5)$$

when $(n-1)U < \mu_{\mathbf{r}} < nU$. Since $E_{0,n+1}(\mathbf{r}) - E_{0,n}(\mathbf{r}) = nU - \mu_{\mathbf{r}}$, the change from a Mott shell with filling fraction n to $n+1$ occurs at the degeneracy condition $\mu_{\mathbf{r}} = nU$, which for a spherically symmetric potential happens at the radius

$$R_{c,n} = a\sqrt{\Omega_n/\Omega}, \quad (6)$$

where $\Omega_n = 2(\mu - nU)$. The relation $\mu_{\mathbf{r}} = nU$ determines the shape and size of the boundary between the n and $n+1$ shells. For instance, in the case of the anisotropic potential of Eq. 2 the same condition leads to ellipsoidal shells

$$\left(\frac{\rho}{a_\rho}\right)^2 + \left(\frac{z}{a_z}\right)^2 = 1 \quad (7)$$

with principal axes $a_\rho = a\sqrt{\Omega_n/\Omega_\rho}$, and $a_z = a\sqrt{\Omega_n/\Omega_z}$. However, near this region of degeneracy, fluctuations due to hopping introduce superfluid shells, as discussed next.

A. Continuum approximation

In this section, we show how the hopping term in Eq. (3) affects the ground state energy of the system. Qualitatively one can see that the kinetic energy controlled by t lifts the degeneracy of the system at $\mu_{\mathbf{r}} = nU$ and in the process introduces a superfluid order parameter in a region of finite width depending on parameters n, t, Ω and U .

To obtain analytical insight into the emergence of superfluid shells, we make first a continuum approximation through the Taylor expansion

$$\psi(\mathbf{r} + \mathbf{a}) = \psi(\mathbf{r}) + a_i \partial_i \psi(\mathbf{r}) + \frac{1}{2} a_i a_j \partial_i \partial_j \psi(\mathbf{r}), \quad (8)$$

where repeated indices indicate summation. This should be true in the limit where the order parameter is smoothly varying at a length scale much greater than the unit lattice spacing a . Under this approximation the effective local Hamiltonian becomes

$$H_{\mathbf{r}}^{\text{eff}} = H_{0,n}(\mathbf{r}) - c_{\mathbf{r}} \Delta^*(\mathbf{r}) - c_{\mathbf{r}}^\dagger \Delta(\mathbf{r}) + \Lambda(\mathbf{r}) \quad (9)$$

where $\Delta(\mathbf{r}) = zt\psi(\mathbf{r}) + ta^2\nabla^2\psi(\mathbf{r})$ reflects the amplitude for the creation of a single boson excitation at position \mathbf{r} , while the last term

$$\Lambda(\mathbf{r}) = \frac{1}{2}[\Delta(\mathbf{r})\psi^*(\mathbf{r}) + \Delta^*(\mathbf{r})\psi(\mathbf{r})] \quad (10)$$

reflects the local mean-field energy shift. Here $z = 2d$ is the number of nearest-neighbor sites (coordination number) depending on the lattice dimension d . Within this approximation, a simple analytical treatment of the emergence of superfluid shells is possible, as discussed next.

B. Nearly Degenerate Perturbation Theory

We focus our attention now on the Mott regions with integer boson filling n and $n+1$ and the superfluid shell that emerges between them. In the limit where $U \gg t$ we can restrict our Hilbert space to number-basis states $|n\rangle$ and $|n+1\rangle$ at each site. Any contribution of other states to the local energy will be of the order of t^2/U . The hopping term in Eq. (3) affects the ground state energy of the system by removing the local degeneracy of $E_{0,n+1}(\mathbf{r})$ and $E_{0,n}(\mathbf{r})$ at $\mu_{\mathbf{r}} = nU$. To illustrate this point, we use the continuum approximation described above and write the Hamiltonian in Eq. 9 in the matrix form

$$H_{\mathbf{r}}^{\text{eff}} = \begin{pmatrix} E_{0,n}(\mathbf{r}) + \Lambda(\mathbf{r}) & -\sqrt{n+1}\Delta(\mathbf{r}) \\ -\sqrt{n+1}\Delta^*(\mathbf{r}) & E_{0,n+1}(\mathbf{r}) + \Lambda(\mathbf{r}) \end{pmatrix}, \quad (11)$$

where $\Delta(\mathbf{r})$ and $\Lambda(\mathbf{r})$ is defined in Eq. 10. Notice that $t \neq 0$ has two effects. First, it changes the local energies $E_{0,n}(\mathbf{r})$ and $E_{0,n+1}(\mathbf{r})$ of the Mott shells n and $n+1$ through $\Lambda(\mathbf{r})$. Second, it mixes the two Mott regions through the off-diagonal term $\sqrt{n+1}\Delta(\mathbf{r})$ and its hermitian conjugate. Thus, the physics near the boundary between the n and $n+1$ Mott regions is described by an effective local two-level system with diagonal ($\Lambda(\mathbf{r})$) and off-diagonal ($\sqrt{n+1}\Delta(\mathbf{r})$) perturbations.

The eigenvalues of Eq. (11) are given by,

$$E_{\pm}(\mathbf{r}) = E_s(\mathbf{r}) \pm \sqrt{(E_d(\mathbf{r}))^2 + (n+1)|\Delta(\mathbf{r})|^2}, \quad (12)$$

where $E_s(\mathbf{r}) = [E_{0,n+1}(\mathbf{r}) + E_{0,n}(\mathbf{r})]/2 + \Lambda(\mathbf{r})$ is proportional to the sum of the diagonal terms, and $E_d(\mathbf{r}) = [E_{0,n+1}(\mathbf{r}) - E_{0,n}(\mathbf{r})]/2 = (nU - \mu_{\mathbf{r}})/2$ is proportional to their difference. These local eigenvalues are illustrated schematically in Fig. 2, where the local energies $E_{0,n}(\mathbf{r})$ and $E_{0,n+1}(\mathbf{r})$ are shown together with the eigenvalues $E_{\pm}(\mathbf{r})$. The radii $R_{n,\pm}$ indicated in the figure correspond to the locations where $\Delta(\mathbf{r}) = 0$.

Notice that $E_-(\mathbf{r})$ is the lowest local energy, leading to the ground state energy $E = \frac{1}{L^d} \int d\mathbf{r} E_-(\mathbf{r})$, where L is the characteristic linear dimension of the system.

The order parameter equation (OPE) is determined by minimization of E with respect to $\psi^*(\mathbf{r})$ leading to

$$\Delta(\mathbf{r}) - \frac{(n+1)t(z + a^2\nabla^2)\Delta(\mathbf{r})}{2\sqrt{|E_d(\mathbf{r})|^2 + (n+1)|\Delta(\mathbf{r})|^2}} = 0. \quad (13)$$

Notice that the OPE is not of the Gross-Pitaevskii (GP) type, since the superfluid regions emerge from local fluctuations between neighboring Mott shells. The zeroth

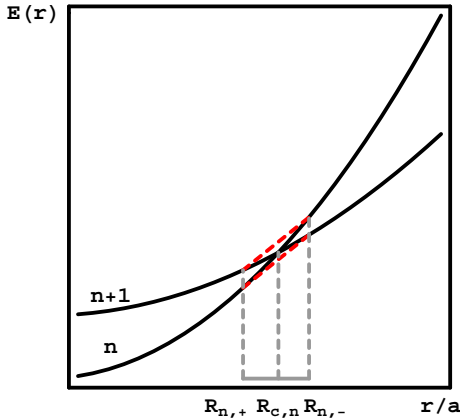


FIG. 2: (Color online) Schematic plot of local energies $E_{0,n}(\mathbf{r})$ and $E_{0,n+1}(\mathbf{r})$ showing the degenerate radius $R_{c,n}$. This local energy degeneracy is lifted by the presence of a finite hopping t , which leads to an avoided level crossing shown as dashed dark-grey (red) curve, and to the emergence of a superfluid region with inner radius $R_{n,-}$ and outer radius $R_{n,+}$

order solution of this equation with $\Delta(\mathbf{r}) = zt\psi(\mathbf{r})$ leads to the spatially dependent order parameter

$$|\psi(\mathbf{r})|^2 = \frac{n+1}{4} - \frac{(nU - \mu_{\mathbf{r}})^2}{4z^2t^2(n+1)}. \quad (14)$$

Since $|\psi(\mathbf{r})|^2 \geq 0$, it implies that $|nU - \mu_{\mathbf{r}}| \leq (n+1)zt$ in the superfluid region. Thus the inner radius $R_{n,-}$ and the outer radius $R_{n,+}$ of the superfluid shell between the n and $n+1$ Mott regions is obtained by setting $|\psi(\mathbf{r})|^2 = 0$ leading to

$$R_{n,\pm} = R_{c,n} \sqrt{1 \pm \frac{2zt(n+1)}{\Omega} \frac{a^2}{R_{c,n}^2}}. \quad (15)$$

for a spherically symmetric harmonic potential $V(r) = \Omega(r/a)^2/2$, where $R_{c,n}$ is defined above. Our notation to describe the Mott-superfluid boundaries is illustrated in Fig. 3.

Equation 15 shows explicitly that t splits the spatial degeneracy of the n and $n+1$ Mott shells at $r = R_{c,n}$ (or $\mu_{\mathbf{r}} = nU$) by introducing a superfluid region of thickness

$$\Delta R_n = R_{n,+} - R_{n,-}. \quad (16)$$

In the case of non-spherical harmonic potential $V(r) = \Omega_{\rho}(\rho/a)^2/2 + \Omega_z(z/a)^2/2$ the shell regions are ellipsoidal instead of spherical. Notice that ΔR_n depends strongly on filling fraction n , the ratio zt/Ω and the chemical potential μ through $R_{c,n}$.

In addition, the local filling fraction

$$n(\mathbf{r}) = -\frac{\partial E_-(\mathbf{r})}{\partial \mu} = n + \frac{1}{2} - \frac{nU - \mu_{\mathbf{r}}}{2zt(n+1)} \quad (17)$$

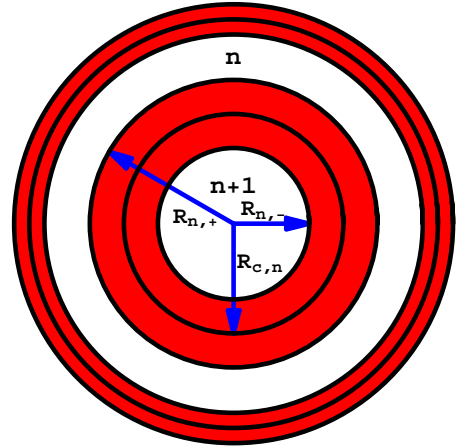


FIG. 3: (Color online) Schematic plot of superfluid regions, shown in gray (red), and the Mott regions, shown in white. The radius $R_{c,n}$ separates Mott shells with filling factor n and $n+1$ for $t = 0$. The superfluid regions have inner radius $R_{n,-}$ and outer radius $R_{n,+}$ and emerge between Mott shells n and $n+1$ for non-zero t .

in the same region interpolates between $n+1$ for $r \lesssim R_{n,-}$ and n for $r \gtrsim R_{n,+}$, while the chemical potential μ is fixed by the total number of particles $N = \int d\mathbf{r} n(\mathbf{r})$.

In Fig. 4, $n(\mathbf{r})$, $|\psi(\mathbf{r})|^2$, and $R_{n,\pm}$ are shown for the Mott and superfluid regions, for $t = 1.25 \times 10^{-2}U$, and $\Omega = 6 \times 10^{-6}U$, and $\mu = 2.5U$. For these parameters, three Mott and three superfluid shells emerge. It is very important to emphasize that in the superfluid regions the order parameter $|\psi(\mathbf{r})|^2$ is not identical to $n(\mathbf{r})$ since the OPE equation is not of the Gross-Pitaevskii type. While the order parameter $\psi(\mathbf{r})$ vanishes at the boundaries $R_{n,\pm}$ between the superfluid and Mott shells, and reaches the maximum value $|\psi(\mathbf{r})|_{max}^2 = (n+1)/4$, when $\mu_{\mathbf{r}} = nU$, the average particle density $n(\mathbf{r})$ interpolates harmonically between Mott shells $n+1$ and n , having the average value of $n+1/2$ when $\mu_{\mathbf{r}} = nU$. Furthermore, we show in Fig. 5 that when $t = 1.25 \times 10^{-2}U$, and $\Omega = 6 \times 10^{-6}U$, and $\mu = 2.2U$ the central shell is superfluid, and the order parameter has a local minimum at the origin of the harmonic trap. As μ increases, this minimum is reduced to zero at a critical value, and the $n = 3$ Mott shell emerges. This property of the emergence of a Mott shell from the center of the trap by suppressing the superfluid order parameter at that region is a generic feature, and can be inferred directly from the phase diagram of Fig. 1 via the substitution $\mu \rightarrow \mu_{\mathbf{r}}$.

The local compressibility

$$\kappa(\mathbf{r}) = \frac{\partial n(\mathbf{r})}{\partial \mu} = \frac{1}{2zt(n+1)} \quad (18)$$

of the superfluid shells is non-zero, in contrast to the incompressible ($\kappa = 0$) n and $n+1$ Mott shells for $r < R_{n,-}$ and $r > R_{n,+}$, respectively. The local compressibility indicates the presence of large (small) excitation energies in the Mott (superfluid) regions, as discussed later.

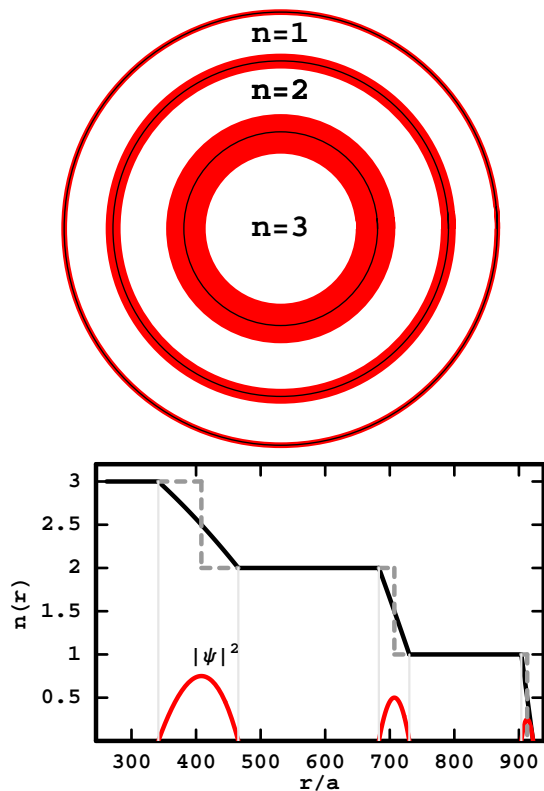


FIG. 4: (Color online) a) Shell structure of Mott and superfluids regions in a 2D square optical lattice with harmonic envelope as a function of radius r/a for $t \neq 0$. The superfluid regions are shown in red (gray) whereas the Mott regions are shown in white. The black circles indicate the Mott boundaries $R_{c,n}$ at $t = 0$. b) The local filling factor $n(r)$ is shown in solid lines for $t \neq 0$ and in dashed lined for ($t = 0$). The red curve (solid gray) shows the local superfluid order parameter $|\psi(\mathbf{r})|^2$. The parameters are $\Omega = 6 \times 10^{-6}U$, $t = 1.25 \times 10^{-2}U$ and $\mu = 2.5U$.

We note that only near the edges of the superfluid region (where $r \approx R_{n,\pm}$ and $\psi(\mathbf{r}) \approx 0$) a direct expansion of the OPE (Eq. 13) leads to the effective Gross-Pitaevskii equation

$$\left(-\frac{1}{2m_{\text{eff}}}\nabla^2 + V_{\text{eff}}(\mathbf{r}) + g_{\text{eff}}|\psi(\mathbf{r})|^2 \right) \psi(\mathbf{r}) = 0. \quad (19)$$

Here, $\hbar = 1$, $m_{\text{eff}} = 1/2a^2t$ is exactly the boson band mass due to the optical lattice, $V_{\text{eff}}(\mathbf{r}) = |nU - \mu_{\mathbf{r}}|/(n+1) - zt$ is the effective potential, and $g_{\text{eff}} = 2zt/(n+1)$ is the effective interaction. Notice that $V_{\text{eff}}(\mathbf{r}) \leq 0$ and vanishes at the boundaries $R_{n,\pm}$ of the superfluid region since $|nU - \mu_{\mathbf{r}}| = zt(n+1)$ there. Furthermore, $g_{\text{eff}} = zt/(n+1)$ is small in comparison to U , indicating that the superfluid near the edges is weakly interacting, and more so as the Mott index n increases. When $t \rightarrow 0$ ($m_{\text{eff}} \rightarrow \infty$) then $|\psi(\mathbf{r})|^2 = -V_{\text{eff}}/g_{\text{eff}}$ leading to the correct limiting behavior of Eq. 13 near $r \approx R_{n,\pm}$.

As discussed above, our nearly degenerate perturbation theory method provides a good description of the

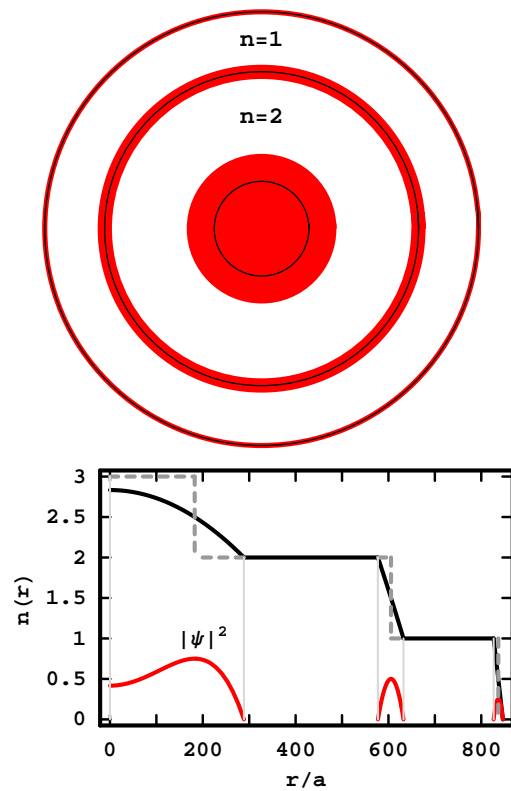


FIG. 5: (Color online) a) Shell structure of Mott and superfluids regions in a 2D square optical lattice with harmonic envelope as a function of radius r/a for $t \neq 0$. The superfluid regions are shown in red (gray) whereas the Mott regions are shown in white. The black circles indicate the Mott boundaries $R_{c,n}$ at $t = 0$. b) The local filling factor $n(r)$ is shown in solid lines for $t \neq 0$ and in dashed lined for ($t = 0$). The red curve (solid gray) shows the local superfluid order parameter $|\psi(\mathbf{r})|^2$. The parameters are $\Omega = 6 \times 10^{-6}U$, $t = 1.25 \times 10^{-2}U$ and $\mu = 2.2U$.

emergence of superfluid shells. This method is a generalization of the perturbation theory developed in [11, 12] for the uniform case, which was believed not to be extendable to describe the emergence of superfluid in harmonically confined optical lattices [14]. Our method, described above and in [8], which relies on direct diagonalization of an effective two level system, thus provides the connection between the mean-field pseudo-spin picture described in [14], and the perturbative approach described in [12].

Next, to clarify when the standard theory developed in [11, 12] breaks down, we compare the results from our nearly-degenerate perturbation theory with the non-degenerate case.

C. Non-degenerate perturbation theory

When the local energies for Mott phase n with energy $E_{0,n}(\mathbf{r}) = Un(n-1)/2 - \mu_{\mathbf{r}}n$, and Mott phase $n+1$ with

energy $E_{0,n+1}(\mathbf{r}) = U(n+1)n/2 - \mu_{\mathbf{r}}(n+1)$, are away for the degeneracy region $\mu_{\mathbf{r}} = nU$, then the correction to the local energy $E_{0,n}$ is

$$E_n^{(2)} = \sum_{m \neq n} \frac{|\langle n|V|m\rangle|^2}{E_{0,n} - E_{0,m}}, \quad (20)$$

where $|m\rangle$ denotes the unperturbed wave function of the excited state with eigenvalue $E_{0,m}$. Here, $V = -c_{\mathbf{r}}\Delta^*(\mathbf{r}) - c_{\mathbf{r}}^\dagger\Delta(\mathbf{r})$ couples only to states with one more or one less atom than in the ground-state, and represents the perturbation to the Hamiltonian $H_{0,n}(\mathbf{r})$ defined in Eq. 4. The fourth order correction can also be calculated using higher-order perturbation theory [12], and leads to the Ginzburg-Landau energy

$$E_n = a_0 + \Lambda(\mathbf{r}) + a_2|\Delta(\mathbf{r})|^2 + a_4|\Delta(\mathbf{r})|^4, \quad (21)$$

The coefficients a_0 , a_2 and a_4 are all functions of parameters $n, U, \mu_{\mathbf{r}}$, and t . The term a_0 corresponds to the unperturbed energy $E_{0,n}(\mathbf{r})$ described in Eq. 5 and associated with the unperturbed Hamiltonian $H_{0,n}$ defined in Eq. 4, while $\Lambda(\mathbf{r})$ is the energy shift shown in Eqs. 9 and 10, which contains spatial derivatives of the order parameter field $\psi(\mathbf{r})$.

The second order coefficient

$$a_2 = \frac{n}{U(n-1) - \mu_{\mathbf{r}}} + \frac{n+1}{\mu_{\mathbf{r}} - Un} + \frac{1}{zt}, \quad (22)$$

determines the existence of superfluid regions, when $a_2 < 0$, while the fourth order coefficient

$$\begin{aligned} a_4 = & \frac{n(n-1)}{[U(n-1) - \mu_{\mathbf{r}}]^2 [U(2n-3) - 2\mu_{\mathbf{r}}]} \\ & + \frac{(n_{\mathbf{r}}+1)(n+2)}{[\mu - Un]^2 [2\mu_{\mathbf{r}} - U(2(n+1))]} \\ & - \left(\frac{n}{U(n-1) - \mu_{\mathbf{r}}} + \frac{n+1}{\mu_{\mathbf{r}} - Un} \right) \\ & \times \left(\frac{n}{(U(n-1) - \mu_{\mathbf{r}})^2} + \frac{n+1}{(\mu_{\mathbf{r}} - Un)^2} \right) \end{aligned} \quad (23)$$

is always positive and is essentially identical to the homogeneous non-degenerate limit [12] except for the replacement of $\mu \rightarrow \mu_{\mathbf{r}}$. However, the inherent inhomogeneity of the trap potential manifest itself in the local energy for the superfluid regions (Eq. 21) through the spatial dependence of the coefficients a_0, a_2 , and a_n and through the spatial derivatives of $\psi(\mathbf{r})$ contained in $\Lambda(\mathbf{r})$. Thus, we define the local Ginzburg-Landau energy difference $\Delta E_n = E_n - a_0$, which, in terms of the order parameter ψ , becomes

$$\Delta E_n = -ta^2\psi^*\nabla^2\psi + a_2z^2t^2|\psi(\mathbf{r})|^2 + a_4z^4t^4|\psi(\mathbf{r})|^4. \quad (24)$$

Here, we retained only terms up fourth order in ψ , and up to second order in derivatives of ψ .

Minimizing ΔE_n to zeroth order in the spatial derivatives of ψ , leads to

$$|\psi(\mathbf{r})|^2 = -\frac{a_2}{2a_4z^2t^2}, \quad (25)$$

and setting $|\psi(\mathbf{r})| = 0$ (or $a_2 = 0$) leads to the local chemical potential

$$2\mu_{\mathbf{r}}^\pm = U(2n-1) - zt \pm \sqrt{U^2 - 2U(2n+1)zt + z^2t^2}, \quad (26)$$

which determines the inner and outer radii of the Mott shell with filling n , where the order parameter $\psi(\mathbf{r}) = 0$ vanishes. Solving Eq. 26 gives the smaller radius of the Mott shell with filling n ,

$$R_{n,+} = R_{c,n} \sqrt{1 + \frac{2zt(n+1)}{\Omega} \frac{a^2}{R_{c,n}^2}}, \quad (27)$$

and the larger radius

$$R_{n-1,-} = R_{c,n-1} \sqrt{1 - \frac{2ztn}{\Omega} \frac{a^2}{R_{c,n-1}^2}}, \quad (28)$$

calculated to order t^2/U . Here, $R_{n,+} > R_{c,n}$, and $R_{n-1,-} < R_{c,n-1}$, where $R_{c,n}$ radius of the Mott shell with filling n when $t = 0$, as defined in Eq. 6. Notice that the size of the Mott region $\Delta R_{n,Mott} = R_{n-1,-} - R_{n,+}$ always decreases with increasing t from its value $R_{c,n-1} - R_{c,n}$ at $t = 0$, showing that superfluid regions emerge at the expense of shrinking the Mott insulator shells.

The corresponding radii defining the superfluid region between the Mott shells with filling factors n and $n+1$ are precisely $R_{n,+}$ and $R_{n,-}$, where $R_{n,\pm}$ are defined in Eq. 15. Thus, to order t^2/U^2 , the thickness of the superfluid shells ΔR_n is again given by Eq. 16, and we recover the results obtained from our degenerate perturbation theory.

Furthermore, minimization of ΔE_n (Eq. 24) with respect to ψ reduces to the same Gross-Pitaevskii equation described in Eq. 19 near the boundaries $R_{n,+}$ and $R_{n,-}$, where the order parameter $\psi(\mathbf{r})$ vanishes. The mapping near the boundaries is $a^2t \rightarrow 1/2m_{\text{eff}}$, $a_2z^2t^2 \rightarrow V_{\text{eff}}(\mathbf{r})$, and $a_4z^4t^4 \rightarrow g_{\text{eff}}$.

In Fig. 6 we compare the results of the non-degenerate perturbation theory with that of our nearly degenerate perturbation theory for small values of t/U . The parameters used are same as in Fig. 4 and we show the results only for the innermost superfluid shell, between $n = 2$ and $n = 3$ Mott shells. Notice that the non-degenerate perturbation theory is correct only very close to the boundaries between the superfluid and Mott regions where $\psi(\mathbf{r})$ is small, but fails to describe the superfluid phase at the center of the superfluid shell corresponding to the degeneracy region.

Having, discussed the non-degenerate perturbation approach and its breakdown, we analyze next the excitation spectrum in the Mott and superfluids regions.

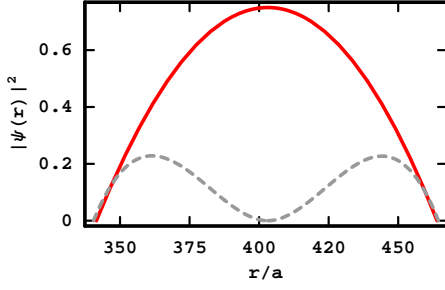


FIG. 6: (Color online) The squared amplitude of the superfluid order parameter $|\psi(\mathbf{r})|^2$ is shown as a solid line (red) for the nearly degenerate case, and as a dashed line (gray) for the non-degenerate case. Notice that near the boundaries where $\psi(\mathbf{r}) \approx 0$, both methods agree and describe the superfluid accurately. However, at the center of the superfluid shell, the non-degenerate method breaks down. The parameters are same as in Fig. 4, and we show the order parameter for the inner most superfluid shell, between $n = 2$ and $n = 3$ Mott shells.

IV. EXCITATIONS IN MOTT AND SUPERFLUID REGIONS

In this section, we discuss relevant excitations in the Mott and superfluid regions, and we use the method of functional integrals to obtain quasiparticle and quasihole excitations in the Mott shells and sound and vortex excitations in the superfluid shells.

A. Quasiparticle and quasihole excitations in the Mott regions

The excitation spectrum in the Mott shells can be obtained using the functional integration method [12] for the action ($\hbar = k_B = 1$, $\beta = 1/T$)

$$S[c^\dagger, c] = \int_0^\beta d\tau \sum_{\mathbf{r}} [c_{\mathbf{r},\tau}^\dagger \partial_\tau c_{\mathbf{r},\tau} + H] \quad (29)$$

leading to the partition function $Z = \int \mathcal{D}c^\dagger \mathcal{D}c \exp(-S[c^\dagger, c])$. In each Mott shell we introduce a Hubbard-Stratonovich field Ψ to take into account fluctuations due to the presence of finite hopping, and integrate out the bosons (c^\dagger, c) leading to an effective action

$$S_{\text{eff}}[\Psi^\dagger, \Psi] = \int d\mathbf{r} \sum_{i\omega, \mathbf{k}, \mathbf{k}'} \Psi_{i\omega, \mathbf{k}} \Psi_{i\omega, \mathbf{k}'}^* e^{i(\mathbf{k}-\mathbf{k}') \cdot \mathbf{r}} G_{\mathbf{k}\mathbf{k}'}^{-1}(i\omega, \mathbf{r})$$

to quadratic order in Ψ^\dagger and Ψ , where \mathbf{k}, \mathbf{k}' are momentum labels, ω are Matsubara frequencies, and

$$G_{\mathbf{k}\mathbf{k}'}^{-1}(i\omega, \mathbf{r}) = \epsilon_{\mathbf{k}'} \left[1 + \epsilon_{\mathbf{k}} \left(\frac{n+1}{i\omega - E_1(\mathbf{r})} - \frac{n}{i\omega - E_2(\mathbf{r})} \right) \right],$$

with $E_1(\mathbf{r}) = nU - \mu_{\mathbf{r}}$, $E_2(\mathbf{r}) = (n-1)U - \mu_{\mathbf{r}}$, and The poles of $G_{\mathbf{k}\mathbf{k}'}(i\omega, \mathbf{r})$ are found upon the analytical

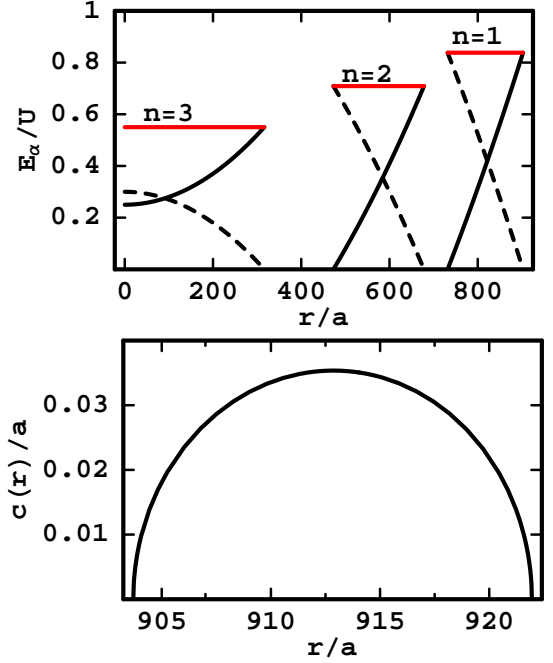


FIG. 7: (Color online) a) Quasiparticle E_{qp} (solid line), quasihole E_{qh} (dashed line), and Mott gap E_g (red) energies for $\mathbf{k} = 0$ versus r/a . b) Sound velocity for the outermost superfluid ring versus r/a . Same parameters as in Fig. 4

continuation $i\omega = \omega + i\delta$, leading to the local excitation energies

$$\omega_{\pm} = -\mu_{\mathbf{r}} + \frac{U}{2}(2n-1) - \frac{\epsilon_{\mathbf{k}}}{2} \pm \frac{1}{2} \sqrt{\epsilon_{\mathbf{k}}^2 - (4n+2)\epsilon_{\mathbf{k}}U + U^2}$$

where the $+$ ($-$) sign labels quasiparticle (quasihole) excitations. The energy to add a quasiparticle is $E_{qp} = \omega_+$, while the energy to add a quasihole is $E_{qh} = -\omega_-$.

Figure 7a shows the quasiparticle and quasihole energies of the Mott phase as a function of position \mathbf{r} . The energy cost to create a quasiparticle (quasihole) is minimum (maximum) at the trap center and increases (decreases) radially, while the Mott-Hubbard gap $E_g = \min_{\mathbf{k}}(E_{qp} + E_{qh})$ is large and independent of \mathbf{r} . Thus, $E_g = \min_{\mathbf{k}} \sqrt{\epsilon_{\mathbf{k}}^2 - 4(n+2)\epsilon_{\mathbf{k}}U + U^2}$, which leads to the final result $E_g = \sqrt{(zt)^2 - 4(n+2)ztU + U^2}$. This expression indicates that it is easier to create a quasiparticle-quasihole excitation inside higher n Mott shells. The horizontal solid (red) line in Fig. 7a also shows this tendency. Since this gap is reduced with increasing n the Mott-insulator gets weaker and thus more susceptible to superfluid fluctuations. Notice that E_g vanishes when $zt/U = (2n+1) \pm 2\sqrt{n(n+1)}$, but the physical solution for the critical value of zt/U corresponds to the largest value, and thus the plus (+) sign.

The large excitation energies in the Mott regions give away to low energy excitations in the superfluid regions as discussed next.

B. Excitations in superfluid regions

While the creation of quasiparticle-quasihole excitations in the Mott regions can be energetically costly, the creation of single quasiparticle excitations, sound waves and vortex excitations in the superfluid shells are more easily accessible.

Single quasiparticle excitations: The single quasiparticle excitation energy can be read off from Eq. 12, since the first excited state of $H_{\mathbf{r}}^{\text{eff}}$ is $E_+(\mathbf{r})$, and the ground state is $E_-(\mathbf{r})$. The local energy difference is $\Delta E = E_+(\mathbf{r}) - E_-(\mathbf{r})$ is independent of \mathbf{r} . This can be seen from the expression $\Delta E = 2\sqrt{|E_d(\mathbf{r})|^2 + (n+1)|\Delta(\mathbf{r})|^2}$, when the approximate result $\Delta(\mathbf{r}) \approx tz\psi(\mathbf{r})$ is used in combination with Eq. 14 and with the definition $E_d(\mathbf{r}) = [E_{0,n+1}(\mathbf{r}) - E_{0,n}(\mathbf{r})]/2 = (nU - \mu_{\mathbf{r}})/2$. The final answer is $\Delta E \approx (n+1)tz$, which indicates that energy cost of adding a quasiparticle in the superfluid shell is small in comparison to the cost of adding a quasiparticle in the Mott region.

It is also interesting to analyze the eigenvectors of the local Hamiltonian defined in Eq. 12. The eigenvector corresponding to E_+ is

$$|E_+\rangle = \begin{pmatrix} \frac{-E_d + \Delta E/2}{\sqrt{n+1}\Delta^*(r)} \\ 1 \end{pmatrix} \quad (30)$$

and reduces to the vector $(0, 1)^T$ corresponding to the energy E_n of the Mott phase with filling n , when $\Delta \rightarrow 0$. The eigenvector corresponding to E_- is

$$|E_-\rangle = \begin{pmatrix} 1 \\ \frac{\sqrt{n+1}\Delta^*(r)}{-E_d - \Delta E/2} \end{pmatrix} \quad (31)$$

and reduces to the vector $(1, 0)^T$ corresponding to the energy E_{n+1} of the Mott phase with filling $n+1$, when $\Delta \rightarrow 0$.

However, the most interesting excitations in the superfluid regions are collective in nature. We will discuss next the collective sound excitations and later the appearance of vortices.

Sound velocity: The excitation spectrum of collective modes in the superfluid region can also be calculated using the functional integral method. First we introduce the Hubbard-Stratonovich field ψ which now corresponds to the order parameter in the superfluid region. Second we use an amplitude-phase representation $\psi(\mathbf{r}, \tau) = |\psi(\mathbf{r}, \tau)| \exp[i\varphi(\mathbf{r}, \tau)]$ and apply the nearly degenerate perturbation theory described earlier to integrate out the boson fields c^\dagger and c . Thus, we obtain the phase-only effective action

$$S_{\text{eff}} = \frac{1}{2L^d} \int d\mathbf{r} d\tau [\kappa(\partial_\tau \varphi)^2 + \rho_{ij} \partial_i \varphi \partial_j \varphi] \quad (32)$$

to quadratic order in the phase variable for the superfluid region between the n and $n+1$ Mott shells. Here,

we assumed that $|\psi(\mathbf{r}, \tau)|$ is τ -independent at the saddle point. The coefficient κ is the compressibility of the superfluid described in Eq. 18, and the local superfluid density tensor

$$\rho_{ij} = \frac{(n+1)ta^2}{2} \frac{F(|\psi|, n, t)}{G(|\psi|, n, t)} - 2ta^2 |\psi|^2 \delta_{ij}, \quad (33)$$

where the numerator of the first term is

$$F(|\psi|, n, t) = t(4z|\psi|^2 \delta_{ij} + 4|\psi|\nabla^2|\psi|\delta_{ij} - 2\partial_i|\psi|\partial_j|\psi|)$$

and the denominator of the first term is

$$G(|\psi|, n, t) = \sqrt{(nU - \mu_{\mathbf{r}})^2/4 + (n+1)t^2\Gamma(|\psi|)},$$

with the function

$$\Gamma(|\psi|) = z^2|\psi|^2 + 2|\psi|\nabla|\psi| + (\nabla^2|\psi|)^2.$$

The complex structure of the superfluid density tensor is a direct consequence of the non-Gross-Pitaevskii nature of the order parameter equation (Eq. 13).

Insight can be gained into the structure of the local superfluid density tensor by neglecting the gradient terms involving $|\psi|$, which in combination with Eq. 14 produces a local superfluid density tensor

$$\rho_s(\mathbf{r}) = \rho_{ii} = 2ta^2|\psi(\mathbf{r})|^2, \quad (34)$$

which vanishes at the Mott boundaries $R_{n,\pm}$. This local superfluid density tensor has been described previously in Refs. [8] and [14], however the more general expression shown in Eq. 33 goes beyond the mean field approximation presented in the pseudo-spin description [14]. In the present approximation, the resulting wave equation has the form

$$\partial_\tau^2 \varphi - \partial_i \left[\frac{\rho_s(\mathbf{r})}{\kappa} \partial_i \varphi \right] = 0, \quad (35)$$

leading to a local sound velocity $c(\mathbf{r}) = \sqrt{\rho_s(\mathbf{r})/\kappa}$, which in terms of the order parameter reads $c(\mathbf{r}) = 2\sqrt{(n+1)zta}|\psi(\mathbf{r})|$. The local speed of sound has its maximum value at $|\psi(\mathbf{r})|_{\text{max}} = (\sqrt{n+1})/2$, and the superfluid region behaves as a medium of continuous index of refraction

$$\chi(\mathbf{r}) = \frac{c_{\text{max}}}{c(\mathbf{r})} = \frac{\sqrt{n+1}}{2|\psi(\mathbf{r})|}. \quad (36)$$

Notice that $\chi(\mathbf{r}) \rightarrow \infty$ at the Mott boundaries where $|\psi(\mathbf{r})| = 0$, indicating that the sound waves of the superfluid do not propagate into the Mott regions. A plot of the local sound velocity is shown in Fig. 7b for the superfluid region between the $n=1$ and $n=0$ Mott shells. From the phase-only effective action for the superfluid region, we can also investigate the vortex excitations, which are discussed next.

Vortices and antivortices: Next, we explore vortex solutions in two cases where spontaneous vortex-antivortex

pairs can appear as indicators of the Berezinski-Kosterlitz-Thouless (BKT) transition [9, 10]. Case I corresponds to a 3D system, where the superfluid regions are very thin $\Delta R_n \ll R_{c,n}$, leading to essentially a two-dimensional superfluid in curved space. Case II corresponds to a 2D system, where the superfluid regions are thick rings $\Delta R_n \sim R_{c,n}$, leading to essentially a two-dimensional superfluid subject to boundary conditions.

In a flat space two-dimensional system stationary vortex solutions must satisfy $\oint \nabla\varphi \cdot d\mathbf{l} = 2\pi m$, where $m = \pm 1, \pm 2, \dots$ is the vorticity (topological charge) and $\nabla\varphi$ is the superfluid velocity. The standard vortex solution in cylindrical coordinates is $\nabla\varphi = m\hat{\theta}/r$, and the corresponding free energy per unit volume is

$$\mathcal{F} = \frac{1}{2L^d} \int d\mathbf{r} \rho_s(\mathbf{r}) (\nabla\varphi)^2. \quad (37)$$

This situation is analogous to a two-dimensional linear dielectric material where the displacement field is

$$\mathbf{D} = \nabla\varphi \times \hat{z} = \epsilon(\mathbf{r})\mathbf{E}, \quad (38)$$

with dielectric function $\epsilon(\mathbf{r}) = 1/[2\pi\rho(\mathbf{r})]$. Notice that the dielectric function diverges at the superfluid boundaries, since $\rho_s(\mathbf{r}) \rightarrow 0$ in those regions. In this language \mathcal{F} is identical to the electrostatic energy per unit volume

$$U_{\text{el}} = \frac{1}{2L^d} \int d\mathbf{r} \mathbf{D} \cdot \mathbf{E}. \quad (39)$$

In general the solutions for several vortices (antivortices) can be obtained from

$$\nabla \wedge \nabla\varphi = 2\pi\hat{z} \sum_i m_i \delta(\mathbf{r} - \mathbf{r}_i), \quad (40)$$

where \mathbf{r}_i is the location of the vortex (or antivortex) of vorticity m_i .

In case I the superfluid state appears below $T_{BKT} \approx \pi\tilde{\rho}_s(\mathbf{r} = \mathbf{R}_{c,n})/2$, where $\tilde{\rho}_s = \rho_s/a^2$ has dimensions of energy. In this limit $\tilde{\rho}_s(\mathbf{r} = \mathbf{R}_{c,n}) = (n+1)t/2$ and the critical temperature of the superfluid shell between the n and $n+1$ Mott regions depends on the index n . Notice, however that such estimate is reasonable only when the radius of the shells are sufficiently large. The solution for a vortex-antivortex (VA) pair in curved two-dimensional space is

$$\varphi(r = R_{c,n}, \theta, \phi) = \arctan \left(\frac{4bR_{c,n} \tan\left(\frac{\pi-\theta}{2}\right) \sin(\phi)}{b^2 - 4R_{c,n}^2 \tan^2\left(\frac{\pi-\theta}{2}\right)} \right)$$

where $R_{c,n} = a\sqrt{2(\mu - nU)/\Omega}$ is the radius of the superfluid shell, and b is the VA size. A three-dimensional view of the velocity field $\nabla\varphi(\theta, \phi)$ is shown in Fig. 8. When the superfluid shell has a small thickness ΔR_n then $T_{BKT} \approx \pi t(n+1)\Delta R_n/6a$, while the vortex-antivortex pair has an approximate solution of the same form as above which interpolates between $\varphi(r = R_{n,-}, \theta, \phi)$ and $\varphi(r = R_{n,+}, \theta, \phi)$.

In case II the superfluid regions are rings bounded by $R_{n,-}$ and $R_{n,+}$, and one can use the Coulomb gas analogy described above, conformal mapping techniques and proper boundary conditions to obtain vortex-antivortex solutions. The creation of vortex-antivortex pairs are energetically quite costly when $\Delta R_n \ll R_{c,n}$, due to strong confinement effects of the boundaries, thus we do not expect a BKT-type superfluid transition to occur until ΔR_n is substantially large ($\sim R_{c,n}$). Only in this limit, we expect a BKT transition with $T_{BKT} \approx \pi\langle\tilde{\rho}_s\rangle/2$, where $\langle\tilde{\rho}_s\rangle/2$ is the surface area average of $\tilde{\rho}_s(\mathbf{r})$.

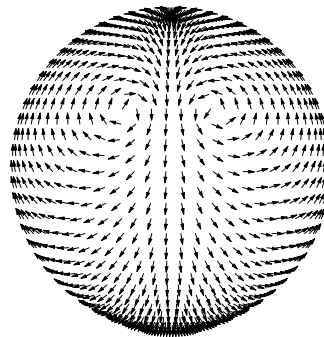


FIG. 8: Three-dimensional view of a vortex-antivortex pair in 2D superfluid shell separating two 3D Mott regions.

Having analyzed the excitation spectra in the insulator and superfluid regions, we discuss next some possible experimental detection schemes for the superfluid shells.

V. DETECTION OF SUPERFLUID SHELLS

Eventhough the use of tomographic microwave techniques has allowed the detection of several Mott regions [5, 6], it has been quite challenging to detect superfluid shells. In this section, we propose a possible experiment for the detection of superfluid shells through the use of Gauss-Laguerre and Gaussian beams followed by Bragg spectroscopy. The idea is that Gauss-Laguerre and Gaussian beams can transfer angular momentum to the atoms in superfluid phase without transferring linear momentum, and that Bragg spectroscopy can detect their existence since the technique is only sensitive to the velocity of the atoms in the superfluid phase. This is because the Mott insulator regions do not absorb the angular momentum because of the presence of a large gap in the excitation spectrum. Next, when the frequencies of the beams used in Bragg spectroscopy are correctly chosen some of the rotating atoms in the superfluid regions acquire extra momentum and are kicked out of their shells and can be imaged.

The Gauss-Laguerre technique has been successfully used to rotate superfluid sodium atoms ^{23}Na in a *mexican hat* potential [15, 16]. The technique used was a two step process, where initially a Gauss-Laguerre beam transferred both linear and angular momentum to atoms,

and a second Gaussian beam canceled the linear momentum transfer leaving each trapped atom with exactly one unit of angular momentum. In this manner, the atoms participating in superfluidity rotate without dissipation, and when the trap is released, the superfluid region expands, but does not fill the center of the cloud, thus maintaining a toroidal structure throughout the time of flight. Furthermore, Bragg spectroscopy was used to detect the sense of rotation of vortices within a vortex lattice of sodium BEC [17] and to observe the persistent flow of Bose-condensed Sodium atoms in toroidal traps [18].

The Gauss-Laguerre technique and Bragg spectroscopy may also be used to detect superfluid shells of bosons in harmonically confined optical lattices. However, the situation here is slightly different because of the existence of Mott shells and multiple superfluid regions. To illustrate this we discuss the simpler case of a nearly two-dimensional configuration, where the harmonic trap is very tight along the z-direction and loose along the x- and y- directions and only two superfluid shells are present. Upon application of the Gauss-Laguerre technique along the z- direction, angular momentum transfer occurs essentially to the atoms in the superfluid phase, imposing a rotating superfluid current with a well defined superfluid velocity profile, while the Mott regions remain unchanged due to their large gap in the excitation spectrum. The angular momentum transfer is chosen to occur along the z direction generating the superfluid currents in the x-y plane, and the amount of angular momentum transfer is assumed to be \hbar for each atom that absorbed a Gauss-Laguerre photon with $l = 1$. Next we use Bragg spectroscopy with counter-propagating beams along the x-direction to detect the sense of rotation and determine the regions of superfluid rings with well defined velocities. If there is sufficient optical resolution and signal-to-noise ratio, then the experiment may be performed *in situ*, otherwise the Bragg spectroscopic measurements can be performed in time-of-flight.

A schematic plot of the detection of superfluid shells using Bragg spectroscopy can be found in Fig. 9, which shows two superfluid shells rotating counter-clockwise and two counter propagating beams applied along the x direction. As can be seen in Fig. 9 the right(left)-going beam has frequency $\omega(\omega')$ and linear momentum $\mathbf{k}(\mathbf{k}')$. The bose atoms undergo a transition from the internal state with energy ϵ_i to the internal state ϵ_f . In the following analysis, we retain \hbar , instead of setting $\hbar = 1$. Applying momentum conservation, we can easily obtain that the final linear momentum of the atoms in the superfluid region is $\mathbf{p}_f = \mathbf{p}_i + \hbar(k + k')\hat{\mathbf{x}}$, in terms of the initial linear momentum of the photons $\hbar k\hat{\mathbf{x}}$ and $-\hbar k'\hat{\mathbf{x}}$. Thus, the Bragg beams transfer a net linear momentum $\hbar(k + k')\mathbf{x}$ to the atoms which satisfies the energy conservation condition

$$\hbar(\omega - \omega') = \epsilon_f - \epsilon_i - v_x \hbar(k + k') + \frac{\hbar^2(k + k')^2}{2m} \quad (41)$$

In the equation above v_x is the component of the veloc-

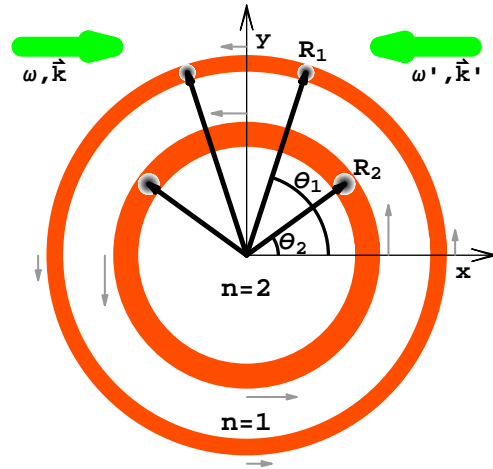


FIG. 9: (Color online) Schematic plot for the detection of superfluid shells using Bragg spectroscopy. The angles θ_1 and θ_2 indicate the locations of strongest momentum transfer from the Bragg beams (large green arrows) to the rotating superfluid shells of radii R_1 and R_2 . The gray arrows indicate the sense of rotation of the superfluid shells.

ity $\mathbf{v}_i = \mathbf{p}_i/m$ along the x direction. Notice that v_x can also be written as $v_x = v_i \sin \theta$ where θ is the angle between the Bragg beams and the velocity \mathbf{v}_i of the atoms in the superfluid shell and $v_i = p_i/m$ is the magnitude of \mathbf{v}_i . For an atom carrying one unit of angular momentum, the superfluid velocity is $\mathbf{v}_i = \hbar\hat{\theta}/mr$. Therefore, within a superfluid shell at position $r = R$ atoms get a linear momentum kick of $\hbar(k + k')\hat{\mathbf{x}}$ when the velocity $v_x = \hbar \sin \theta / mR$ satisfies the condition given in Eq. 41. This leads to two Bragg angles $\theta = -\sin^{-1}(mRv_x/\hbar)$, and $\pi - \theta$ for each superfluid shell. As can be seen in Fig. 9 the Bragg angles are θ_1 and $\pi - \theta_1$ for the outer superfluid shell labelled by R_1 , and are θ_2 and $\pi - \theta_2$ for the inner superfluid shell labelled by R_2 . The regions with same velocity v_x are identified by the condition $\sin \theta_1/R_1 = \sin \theta_2/R_2 = mv_x/\hbar$. Once these atoms are kicked out of their respective superfluid shells, they form two small cloud, which can be detected by direct imaging. As mentioned before, if there is sufficient optical resolution and signal-to-noise ratio, then the experiment may be performed *in situ*, otherwise the Bragg spectroscopic measurements can be performed in time-of-flight. In fact these clouds also carry the information of the sense of rotation of the superfluid shells and their velocity profile, and one can in principal extract that information from the images.

Having discussed our proposal for the experimental detection of superfluid shells in harmonically confined optical lattices, we present next our conclusions.

VI. CONCLUSIONS

We studied 2D and 3D optical lattices of atomic or molecular bosons in harmonically confining potentials, and showed that between the Mott regions of filling fraction n and $n + 1$, superfluid shells emerge as a result of fluctuations due to finite hopping. We found that the presence of finite hopping breaks the local energy degeneracy of neighboring Mott-shells, determines the size of the superfluid regions as shown in Fig 4, and is responsible for low energy (sound) and vortex excitations. In addition, we obtained an order parameter equation which is not in general of the Gross-Pitaevskii type, except near the boundaries separating the super-

fluid from the insulating regions. Furthermore, we obtained bound vortex-antivortex solutions (as shown in Fig 8 below the Berezinski-Kosterlitz-Thouless (BKT) transition when superfluid regions are thin (nearly 2D) spherical (or ellipsoidal) shells. Finally, we discussed that the emergence of these superfluid regions should be detectable using a combination of Gauss-Laguerre and Bragg spectroscopy techniques.

We thank NSF (DMR 0304380, and PHY 0426696) for financial support. We thank F. W. Strauch, E. Tiesinga, C. W. Clark, I. Spielman, W. D Phillips, and K. Helmerson for discussions, and we thank R. A. Barankov, C. Lannert, and S. Vishveshwara for drawing our attention to their related work [14].

-
- [1] Immanuel Bloch, Nature Phys. **1**, 23 (2005).
 - [2] Markus Greiner, Olaf Mandel, Tilman Esslinger, Theodor W. Hänsch, and Immanuel Bloch, Nature (London) **415**, 39 (2002).
 - [3] Thilo Stöferle, Henning Moritz, Christian Schori, Michael Köhl, and Tilman Esslinger, Phys. Rev. Lett. **92**, 130403 (2004).
 - [4] I. B. Spielman, W. D. Phillips, and J. V. Porto, Phys. Rev. Lett. **98**, 080404 (2007)
 - [5] Gretchen K. Campbell, Jongchul Mun, Micah Boyd, Patrick Medley, Aaron E. Leanhardt, Luis G. Marcassa, David E. Pritchard, and Wolfgang Ketterle, Science **313** 649 (2006).
 - [6] Simon Fölling, Artur Widera, Torben Mller, Fabrice Gerbier, and Immanuel Bloch, Phys. Rev. Lett. **97**, 060403 (2006).
 - [7] D. Jaksch, C. Bruder, J. I. Cirac, C. W. Gardiner, and P. Zoller, Phys. Rev. Lett. **81**, 3108 (1998).
 - [8] Kaushik Mitra, C. J. Williams, and C. A. R. Sá de Melo, cond-mat/0702156 (2007).
 - [9] V. L Berezinskii, Sov. Phys. JETP **32**, 493 (1971).
 - [10] J. M. Kosterlitz, and D. Thouless, J. Phys. C **5**, L124 (1972).
 - [11] Matthew P. A. Fisher, Peter B. Weichman, G. Grinstein, and Daniel S. Fisher, Phys. Rev. B **40**, 546 (1989).
 - [12] D. van Oosten, P. van der Straten, and H. T. C. Stoof, Phys. Rev.A, **63**, 053601 (2001).
 - [13] N. F. Mott, Proc. Phys. Soc., London, Sect. A **62**, 416 (1949).
 - [14] R. A. Barankov, C. Lannert, S. Vishveshwara, cond-mat/0611126 (2006).
 - [15] M. F. Andersen, C. Ryu, Pierre Cladé, Vasant Natarajan, A. Vaziri, K. Helmerson, and W. D. Phillips, Phys. Rev. Lett. **97**, 170406 (2006).
 - [16] C. Ryu, M. F. Andersen, P. Cladé, Vasant Natarajan, K. Helmerson, W. D. Phillips, cond-mat/0709.0012v1.
 - [17] S. R. Muniz, D. S. Naik, and C. Raman, Phys. Rev. A **73** 041605(R) (2006).
 - [18] K. Helmerson, *private communication*.